Meteorol Atmos Phys (2011) 113:39–53
DOI 10.1007/s00703-011-0145-9

ORIGINAL PAPER

The sensitivity of African easterly waves to eastern tropical Atlantic sea-surface temperatures

Leonard M. Druyan · Matthew Fulakeza

Received: 13 October 2010 / Accepted: 25 May 2011 / Published online: 10 June 2011

Abstract The results of two regional atmospheric model simulations are compared to assess the influence of the eastern tropical Atlantic sea-surface temperature maximum on local precipitation, transient easterly waves and the West African summer monsoon. Both model simulations were initialized with reanalysis 2 data (US National Center for Environmental Prediction and Department of Energy) on 15 May 2006 and extended through 6 October 2006, forced by synchronous reanalysis 2 lateral boundary conditions introduced four times daily. One simulation uses 2006 reanalysis 2 sea-surface temperatures, also updated four times daily, while the second simulation considers ocean forcing absent the sea-surface temperature maximum, achieved here by subtracting 3°K at every ocean grid point between 0° and 15°N during the entire simulation. The simulation with 2006 sea-surface temperature forcing produces a realistic distribution of June–September mean precipitation and realistic westward propagating swaths of maximum rainfall, based on validation against Tropical Rainfall Measuring Mission (TRMM) estimates. The simulation without the sea-surface temperature maximum produces only 57% of the control June–September total precipitation over the eastern tropical Atlantic and about 83% of the Sahel precipitation. The simulation with warmer ocean temperatures generates generally stronger circulation, which in turn enhances precipitation by increasing moisture convergence. Some local precipitation enhancement is also attributed to lower vertical thermal stability above the warm water. The study shows that the eastern tropical Atlantic sea-surface temperature maximum enhances the strength of transient easterly waves and broadens the spatial extent of associated precipitation. However, large-scale circulation and its interaction with the African continent, and not sea-surface temperatures, control the timing and trajectories of the waves.

Responsible editor: J. Fasullo.

L. M. Druyan (✉) · M. Fulakeza
Center for Climate Systems Research, Columbia University and the NASA/Goddard Institute for Space Studies, 2880, Broadway, New York, NY 10025, USA
e-mail: Leonard.M.Druyan@nasa.gov

1 Introduction

The West African monsoon (WAM) rainy season is June–September. Sea-surface temperature anomalies (SSTA) demonstrably influence the interannual variability of the WAM climate according to the combined observational and modeling studies of Folland et al. (1986), Rowell (2001, 2003) and the model study of Giannini et al. (2003). Various mechanisms linking SSTA to precipitation anomalies in the Sahel have been proposed. For example, the seasonal precipitation maximum over the eastern tropical Atlantic and over West Africa is situated several hundred kilometers south of the near-surface wind confluence (Hastenrath and Polzin 2010). Gridded observational analyses show that the wind confluence, in turn, relates to the monsoon pressure trough, which reaches a more northerly latitude during years with positive SSTA in the North Atlantic roughly between 10°N and 20°N (Hastenrath and Polzin 2010). In general, major eastern Atlantic inter-tropical convergence zone (ITCZ) summer rainfall is confined to a band of SSTs greater than 300°K (Xie and Carton 2004). Moreover, the position and strength of the Atlantic ITCZ is sensitive to the strength of the cross-equatorial SST gradient. Whether or not the sensitivity of WAM seasonal rainfall to SSTA is manifest as impacts on

individual transient synoptic (cyclonic) disturbances has not been studied.

Time series of the recorded meridional wind (v) at 850, 700 or 600 mb in the WAM region show periodic variability caused by transient synoptic (cyclonic) disturbances, called African easterly waves (AEWs) with wavelengths of 2,500–4,000 km, based on observational data (Burpee 1972; Reed et al. 1977; Druyan et al. 1996). For convenience, easterly waves traversing the eastern tropical Atlantic are referred to in the current study as AEWs. Xie and Carton (2004) suggest that AEWs act as a dynamic trigger for eastern tropical Atlantic precipitation in July, despite SST decreases of 1°K on average from March to April. Studies show that AEWs can be detected by Fourier spectral analysis of v time series, which reveals spectral peaks at 3- to 6-day periods. Zones of maximum spectral amplitude of v time series or of vorticity variance indicate trajectories of AEWs. For example, Reed et al. (1988) deduce AEW trajectories based on gridded data from ECMWF analyses and forecasts projected on a 3° by 3° latitude–longitude grid by mapping the 700-mb vorticity variance filtered for 2.9–4.0 and 2.9–4.7-day periods. Their analysis is confined to August–September 1985 and show northerly and southerly AEW tracks merging into one along 19°N over the eastern North Atlantic Ocean. Druyan et al. (2009) show the spatial distribution of spectral amplitudes of 700-mb meridional winds ($v7$) for 3- to 6-day periods for a regional model (RM3) September 2006 simulation, which indicates two AEW trajectories, along 5°N at the Gulf of Guinea coast and along 15°N over the eastern tropical Atlantic. Thorncroft and Hodges (2001) track AEW vorticity maxima at 600 and 850 mb over West Africa and the tropical Atlantic Ocean using 20 years of ECMWF analyses with an equivalent horizontal grid of 2.8°. They detect AEW trajectories along 10°–13°N, but their data refer to the entire summer. In any case, there is considerable interannual variability in AEW tracks associated with the WAM (Druyan et al. 2006; Thorncroft and Hodges 2001). Some percentage of AEWs eventually develops into tropical storms and some into Atlantic hurricanes (Ross and Krishnamurti 2007; Hopsch et al. 2010).

Can observed, large departures of WAM summer temperature and precipitation from climatological means be explained in part as sea-surface temperature (SST) impacts on AEWs? Storm tracks derived by Hopsch et al. (2007) from ECMWF 40-year reanalysis data are centered near 11°N over the eastern tropical Atlantic. Their study does not find a correlation between the interannual variability of the number of storm tracks over the tropical Atlantic Ocean and SST anomalies. Hopsch et al. (2010) contrast composite observed SST distributions for developing and non-developing cyclones in the eastern tropical Atlantic Ocean. SST for developing systems are up to 1.8°C warmer adjacent to the West African coast near 20°N, but this is north of the area of usual cyclone development. Hopsch et al. (2010) suggest, however, that the warmer SST may favor cyclogenesis by influencing air that is converging toward developing low centers. Woolings et al. (2010) find that regional model simulations of extratropical Atlantic cyclone storm tracks show some sensitivity to both the spatial and temporal resolution of specified SST. At least one study shows that the position of maximum convective activity, associated with the ITCZ over the tropical Atlantic Ocean, depends on SST gradients (Chiang et al. 2002). Presumably, therefore, daily rainfall rates are sensitive to SSTA. Warm water can destabilize the atmosphere, enhance convective precipitation and promote upward water vapor flux that feeds the developing cumulus, while cold SSTA can inhibit moist convection. Given the importance of moist convection to a tropical storm's energy budget, what impact do SSTA have on a developing or intensifying AEW over the eastern tropical Atlantic? Are these impacts manifest as changes in the spectral signatures of $v7$ time series along AEW trajectories? Are the wave intensities or periodicities sensitive to SSTA?

Thorncroft et al. (2007) discuss the trajectories of AEWs and intraseasonal variability of the WAM during June–September 2006, coinciding with the AMMA (African Monsoon Multidisciplinary Analysis) special observing periods, and also the time frame of the current study. Based on the analyzed 700-mb curvature vorticity (averaged between 5° and 15°N), they find that in July 2006, most AEWs form near 0° longitude, while in August they are initiated further east, between 10° and 20°E. Moreover, from the end of August and into September, AEWs become more coherent, with stronger amplitudes over most of tropical North Africa. Interestingly, several AEWs also appear to start further east, between 20° and 30°E, at this time. AEWs can serve as the seeds for tropical cyclones. Thorncroft et al. (2007) note that all seven of the 2006 AEWs that become named tropical cyclones are initiated east of Niamey (13°N, 2°E) and six of these occur after the middle of August.

Recent regional atmospheric model experiments of the September 2006 climate (Druyan et al. 2009) show that convective precipitation over the southeastern North Atlantic between 5°and 8°N is sensitive to the vertical thermal instability above the warmest SSTs. In Druyan et al. (2009), however, large-scale upward vertical motion north of 9°N is associated more with transient cyclonic disturbances, contributing to rainfall occurring north of the mean ITCZ. In that study, cumulus heating rate peaks within a tropical depression rain shield are reduced by about 30% by prescribing −3°K SSTA between 0° and 15°N. They are also marginally enhanced by warm SSTA. The present study investigates the influence of the tropical

Atlantic SST maximum on the WAM and adjacent Atlantic summer climate and on AEWs.

2 Experiment design

Druyan et al. (2006, 2008) describe the regional climate model (3rd generation version) used in this study (hereafter RM3). The model is integrated on a horizontal grid with 0.5° latitude/longitude spacing at 28 vertical sigma levels. Ground temperatures are simulated internally using the land surface (LS) process model developed for the GISS GCM (Rosenzweig and Abramopoulos 1997; Hansen et al. 2002). The LS model consists of two integrated parts, the soil and the canopy, and it conserves water and heat while simulating their vertical fluxes. The RM3 modeled soil is divided into six layers to a depth of 3.5 m, and the model distinguishes between five textures of soil. The canopy, modeled as a separate layer located above the soil, is responsible for the interception of precipitation, evaporation of accumulated water and removal of soil water through transpiration. Ocean temperatures are specified boundary data that are updated daily. The Del Genio and Yao (1993)moist convection parameterization and the Del Genio et al. (1996) scheme for the effects of cloud liquid water are also incorporated into the RM3. The cloud liquid water scheme allows for life cycle effects in stratiform clouds and permits cloud optical properties to be determined interactively.

The domain for simulations is 20°S–35°N, 50°W–20°E, which represents a westward shift of 15° relative to the domain used by Druyan et al. (2009), but the 0.5° grid spacing is retained. The shift creates a domain better suited for studies over the Atlantic. Two simulation experiments are conducted to evaluate the sensitivity of WAM and eastern tropical Atlantic climate to the SST maximum in the eastern tropical Atlantic Ocean. Both are driven with atmospheric data from the US National Center for Environmental Prediction and Department of Energy reanalysis 2 (NCPR2) (Kanamitsu et al. 2002) for 15 May–6 October 2006, but most results focus on June–September (JJAS). NCPR2 data are archived on grids with 2.5° latitude/longitude spacing and applied synchronously four times per day at the lateral boundaries of the RM3 domain. The downscaling of NCPR2 reanalysis to the RM3 0.5° grid allows more spatial detail of meteorological variables and land surface conditions to be considered in the integration of simulations and the presentation of results. The May part of the simulations serves as a spin-up. To compute spectra, simulated time series are required to extend to 6 October. The basic RM3 simulation, hereafter RM3c, is forced with compatible NCPR2 SST for 2006.

In the second simulation, SSTs are altered to eliminate the tropical SST maximum east of 50°W. A constant 3.0°K is subtracted from the NCPR2 2006 SST values at every time step, between the equator and 15°N, which is the swath of maximum SST in the eastern tropical North Atlantic Ocean. This configuration is only one of different possible SST specifications that eliminate the maximum, but it was the one used by Druyan et al. (2009). A 3.0°K anomaly of the monthly mean SST over broad tropical ocean areas is, however, at the high end of naturally occurring events. Note that the SSTA are imposed under the main storm track of the tropical Atlantic (Hopsch et al. 2007). The cold SSTA simulation experiment is hereafter referred to as RM3ca. Figure 1 shows SST distributions for JJAS 2006 and for RM3cA. Imposing uniform −3°K anomalies creates unrealistically sharp SST gradients at the equator and at 15°N. The alternative of imposing a more complex pattern with vanishing SST gradients was not selected. The gradients in the chosen configuration did not cause any unrealistic meteorological repercussions to the simulation.

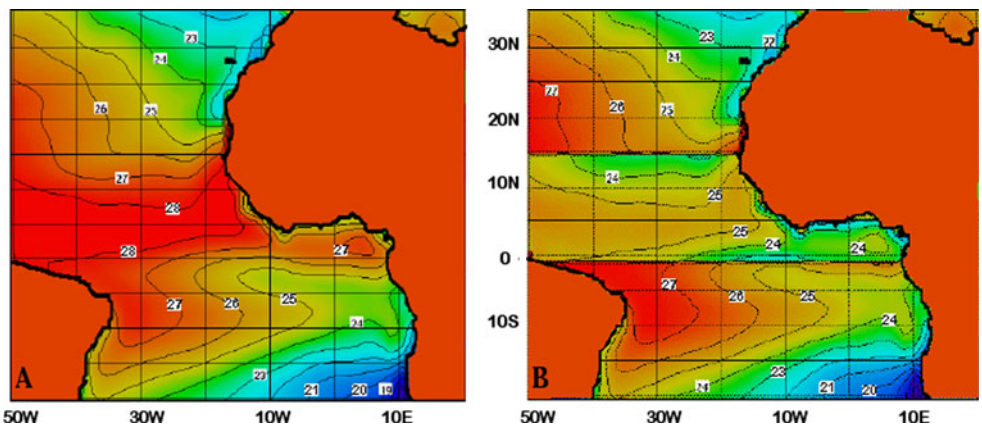

Fig. 1 Sea-surface temperature distributions for JJAS: **a** 2006; **b** RM3ca experiment

3 SST impacts on seasonal and daily precipitation

3.1 Simulation of the JJAS 2006 precipitation distribution

Figure 2 shows a map of West Africa that identifies some of the geographical features referred to in the discussion below. Figure 3a shows the TRMM (Tropical Rainfall Measuring Mission) accumulations for JJAS 2006. The RM3 precipitation simulation using observed JJAS 2006 SST boundary conditions (RM3c) is shown in Fig. 3b. Adverse lateral boundary effects distort the simulated precipitation pattern within the westernmost 3° of longitude and easternmost 10°. Otherwise, favorable features include the axis of maximum accumulations aligned realistically along 7°N over the Atlantic and along 11°N over West Africa. The orographic maxima along the coast near the Guinea Highlands and over the Cameroon Highlands are quite realistic. Within the Atlantic ITCZ, RM3 maximum values match TRMM maxima fairly well, but accumulations are about 25% higher than TRMM over broad areas of West Africa. The modeled precipitation gradient on the north side of the Atlantic ITCZ is reasonable, but the gradient on the south side of the ITCZ is too diffuse, with too much rain simulated over the equator. RM3 precipitation is also too generous over the southwestern corner of the figure.

3.2 Impact of SST maximum on JJAS 2006 precipitation

Figure 3c shows RM3c minus RM3ca JJAS 2006 precipitation differences, representing the impact of the Atlantic

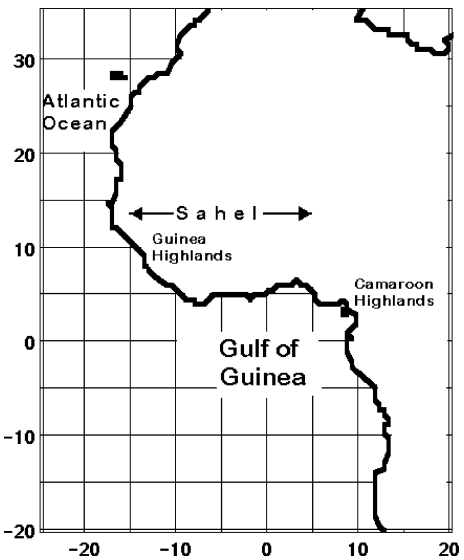

Fig. 2 Map of geographic features discussed in the text

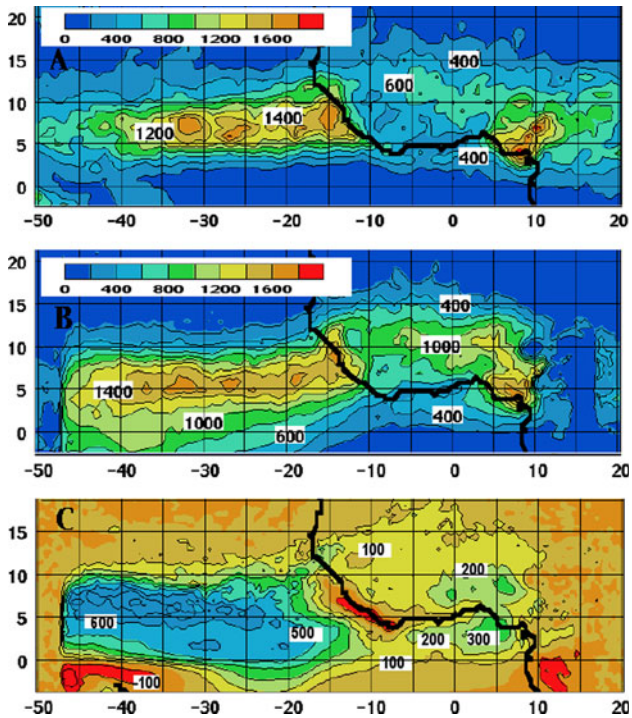

Fig. 3 **a** JJAS 2006 accumulated TRMM precipitation (mm) (courtesy, interactive online visualization and analysis infrastructure, NASA Goddard Earth Sciences, Data and Information Services Center), **b** JJAS 2006 accumulated RM3c precipitation (mm), **c** RM3c minus RM3ca accumulated precipitation (mm)

SST maximum. See also Table 1. As expected, the largest impacts are over the warmest Atlantic water, centered along 6°–8°N, roughly the latitude of the ITCZ. For example, within the area bounded by 6–8°N, 25–35°W, RM3c total seasonal accumulations are about 594 mm (74%) higher than for RM3ca. SST impacts on the accumulated precipitation also extend beyond the equator into the southern hemisphere. Are parallel differences observed in nature? Consider the comparison between JJAS 2009 and 2010, shown in Fig. 4. The average SST over the area 0–10°N, 20–40°W is 1.0°K warmer in JJAS 2010 (based on NCPR2), and TRMM observations of the JJAS 2010 accumulated precipitation in the area 6–8°N, 25–35°W are about 35% higher than for JJAS 2009 (1,631 vs.

Table 1 JJAS total accumulated precipitation, evaporation and $P - E$ for 6°–8°N, 25°–35°W for two simulations, and impacts of the cold anomaly experiment

Simulation	Total precipitation (mm)	Total evaporation (mm)	$P - E$ (mm)
RM3c	1,392	422	970
RM3cA	798	381	417
Impact	−594	−41	−553

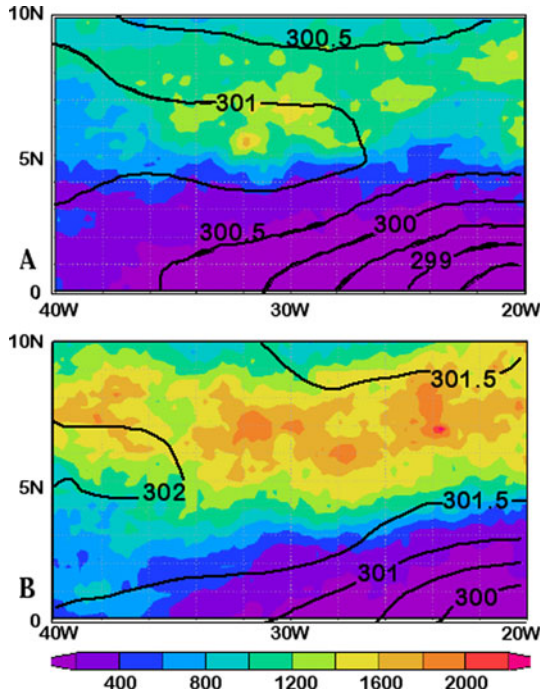

Fig. 4 JJAS sea-surface temperature contours (°K) based on NCEP reanalysis 2 (courtesy NOAA/Earth System Research Laboratory/Physical Science Division) superimposed over TRMM JJAS precipitation accumulations (mm, shaded) (courtesy NASA GES DISC). **a** 2009, **b** 2010

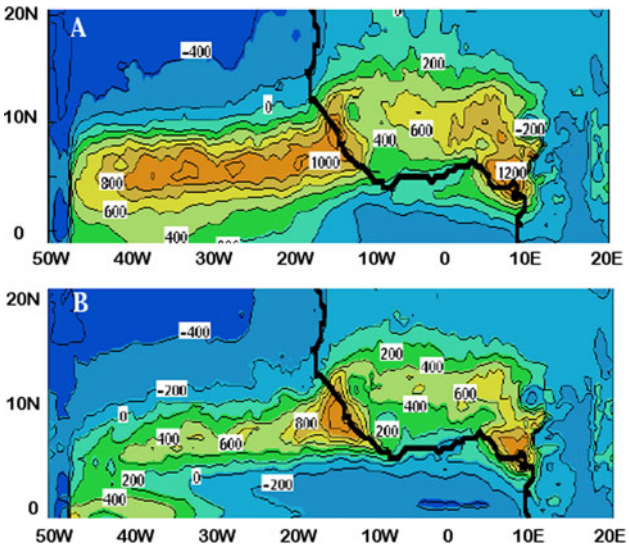

Fig. 5 JJAS precipitation minus evaporation (mm): **a** RM3c; **b** RM3ca

1,205 mm). From this perspective, the simulation results are reasonable.

The mean JJAS precipitation minus evaporation ($P - E$) is a good estimate of the seasonal net moisture convergence. Small $P - E$ implies that the net moisture convergence into an area is near zero, while large $P - E$ implies that the moisture for the precipitation excess is imported from elsewhere. Figure 5a shows $P - E$ for RM3c and Fig. 5b for RM3ca. Maxima in the implied moisture convergence occur over the coast near the Guinea Highlands, over the Cameroon Highlands and within the mean position of the Atlantic ITCZ. AMMA Land-surface Model Intercomparison Project (ALMIP) estimates of $P - E$ for 2003–2005 (Druyan et al. 2010) also show local maxima over the coast near the Guinea Highlands and the Cameroon Highlands. $P - E$ maxima account for about 70% of the RM3c seasonal rainfall (Table 1). Northward moisture advection (not shown) is strongest over the Atlantic between 5°S and 5°N, weakening northward toward the mean Atlantic ITCZ and West Africa, which experience maximum moisture convergence.

Table 1 shows that the RM3c excess in precipitation over the tropical Atlantic relative to RM3ca is consistent with a more than doubling of the moisture convergence ($P - E$). On the other hand, total evaporation increases by only about 10%. Indeed, mass convergence at 925 mb for RM3c within the Atlantic ITCZ is about 33% higher than for RM3ca (not shown).

RM3c excesses in seasonal precipitation over West Africa range between 100 and 300 mm, or about 10–20% of the total, and these impacts are also accounted for by $P - E$, the proxy for moisture convergence. RM3c and RM3ca experience approximately the same JJAS evaporation over West Africa. The smallest positive RM3c impacts and a swath of negative impacts are situated along the coast near the Guinea Highlands within the zone of onshore monsoon circulation. Despite warmer SST, RM3c precipitation is diminished along the windward side of the Guinea Highlands, related perhaps to a less efficient orographic lift and less efficient coastal convergence of the onshore circulation. Indeed, RM3ca $P - E$ is about 10% higher in this location. Time-dependent variations of impact are studied in the next section using Hovmöller distributions of daily rainfall.

3.3 Time–longitude variability of JJAS 2006 precipitation

Hovmöller time–longitude representations conveniently monitor the westward propagation of precipitation maxima associated with AEWs. Figure 6a, b compares the TRMM and RM3c daily precipitation, averaged over 5°–15°N, for each day of JJAS 2006. While some swaths begin as far east as 10°E, other swaths are initiated closer to 10°W. Thorncroft et al. (2007) made a similar observation regarding 2006 AEWs based on time–longitude diagrams of AEW curvature vorticity. Note that the simulated precipitation maxima in Fig. 6b matches the time and location of most TRMM observed maxima (Fig. 6a), although

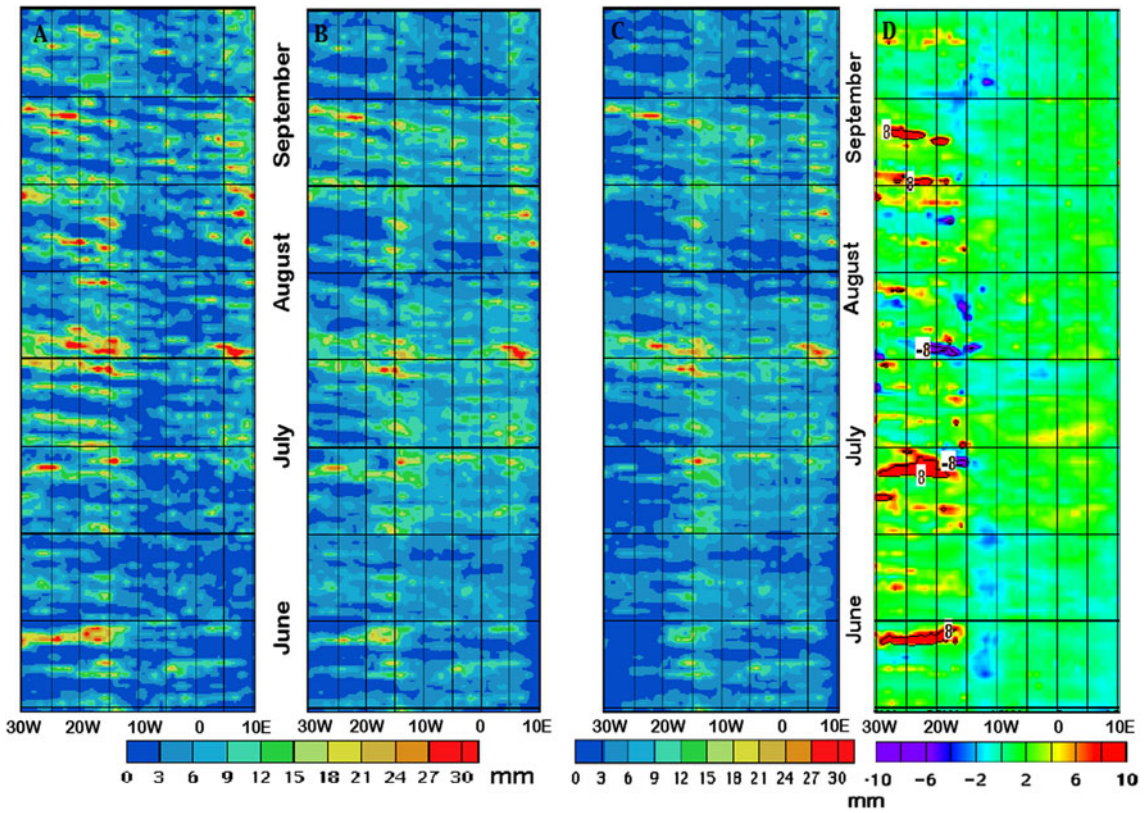

Fig. 6 Time–longitude distributions of daily precipitation (mm) averaged over 5°–15°N for JJAS 2006: **a** TRMM (courtesy, NASA GES DISC), **b** RM3c, **c** RM3ca, **d** RM3c minus RM3ca

TRMM maximums are consistently higher. In addition, the RM3 simulates less extensive areas/events of precipitation under 3 mm.

Statistics comparing model versus TRMM data in Fig. 6a, b are given in Table 2 for monthly sections: June, July, August and September. Time–space correlations range from 0.70 to 0.86, while the correlation over the entire period is 0.77, all statistically significant at the 99% confidence level. July shows the lowest correlation and the most extreme bias. The standard deviation of model simulated precipitation is lower than for TRMM in every month, reaching only 65–71% of TRMM values. This means that model maxima are consistently underestimated relative to TRMM, while very low values are not generated often enough, as can be seen by comparing Fig. 6a, b.

Table 2 Statistics comparing RM3c time–longitude Hovmöller daily precipitation distributions with corresponding TRMM data, daily 1 June–30 September 2006

Month/statistic	Corr. coeff.	RM3 bias (mm)	RM3 std. dev.	TRMM std. dev.
June	0.86	+0.7	3.5	5.1
July	0.70	+1.6	4.4	6.4
August	0.76	−0.3	5.0	7.7
September	0.81	−0.6	4.5	6.3

Longitude range is 30°W–10°E and data are averaged over 5°–15°N. All correlations are statistically significant at the 99% confidence level

Figure 6c shows the same Hovmöller time–longitude distribution for the RM3ca experiment and Fig. 6d shows the time versus longitude distribution of precipitation differences, RM3c minus RM3ca. The alternative SST specifications do not alter the timing of the westward moving precipitation maxima, implying no SSTA impact on the movement of AEWs. Warmer SSTs enhance many precipitation maxima, even though they decrease the rainfall of at least two precipitation systems, most notably on 3rd August. The largest impacts are west of 15°W, which means that they occur over the eastern tropical Atlantic Ocean. Despite SST differences in the Gulf of Guinea, the most prominent impacts on daily rainfall rates over West Africa are RM3c increases of about 5 mm day^{-1} at 5°E–5°W on 18–20 July.

Figure 7 shows the section covering the interval 16 August–16 September from the same Hovmöller diagrams as in Fig. 6. It affords a more detailed look at one of the more active periods of the 2006 summer. The RM3c simulation represents all observed precipitation swaths, although modeled amounts have a smaller range than

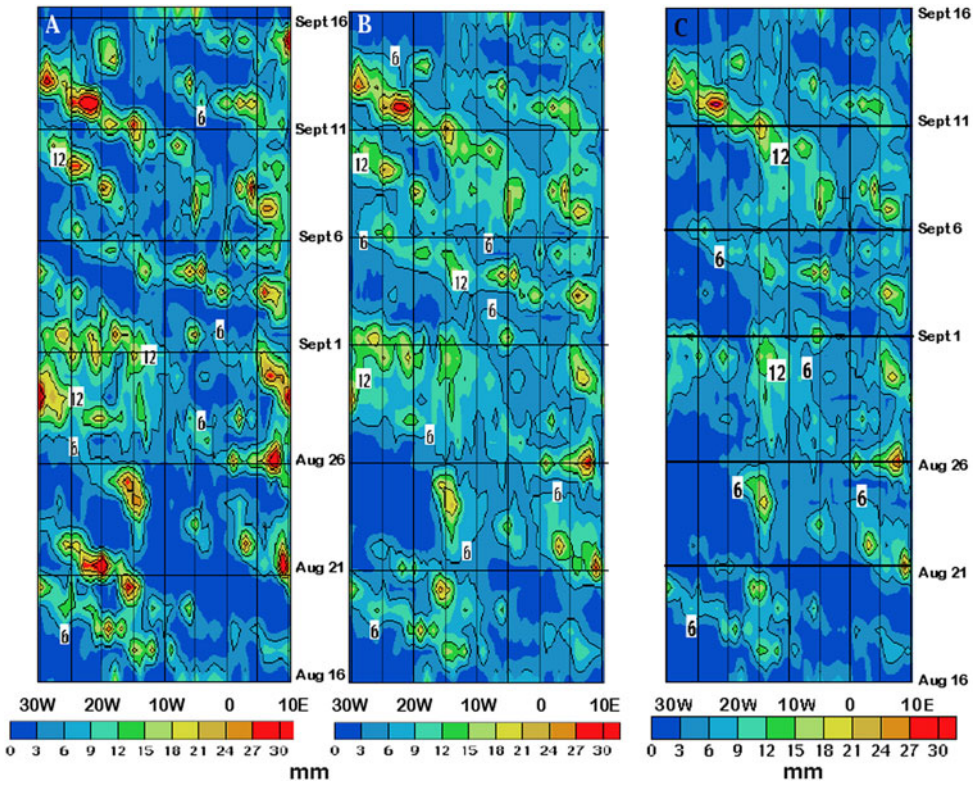

Fig. 7 Time–longitude distributions of daily precipitation (mm) averaged over 5°–15°N, for 16 August–16 September 2006: **a** TRMM (courtesy, NASA GES DISC), **b** RM3c, **c** RM3ca

TRMM. The diagonal swaths of precipitation suggest a westward movement ranging between 3° and 10° longitude per day. Note that the movement of precipitation maxima may not always indicate the propagation speeds of their associated AEWs, since squall lines can move through the waves or otherwise change quadrants. A transient wave, traversing 8–30°W during 10–14 September, includes a precipitation maximum exceeding 40 mm on 12 September, which is simulated by RM3c quite realistically. This event is associated with the development of Tropical Storm Helene. Thorncroft et al. (2007) show a similar pattern of propagating AEWs during JJAS 2006, based on the time–longitude plot of 700 mb curvature vorticity.

The 16 August–16 September Hovmoller segment for experiment RM3ca (Fig. 7c) indicates that the cooler SST generally weaken precipitation maxima, shortening or even eliminating westward propagating systems. The largest impacts occur after the systems traverse the African coastline and move out over the adjacent tropical Atlantic Ocean, but weakened maxima are also discernable at longitudes corresponding to West Africa. The best example of how the presence of the eastern tropical Atlantic SST maximum enhances AEW-related precipitation is the swath through 28°W on 10 September. Warmer SSTs considerably strengthen in situ precipitation associated with this transient AEW.

RM3c minus RM3ca differences in precipitation on any single day cannot be attributed to the contrasting SST forcing with any confidence because of random variability inherent in the computations of convective rainfall. Rather, consistent RM3c enhancement of precipitation swaths throughout JJAS, relative to RM3ca, as shown in Fig. 6, is more reliable evidence of the SST influence. However, it is interesting to see an example of the spatial distribution of precipitation differences associated with AEWs. Figure 8 shows rainfall associated with two AEWs on 10 September 2006. Figure 8a shows the TRMM estimates and Fig. 8b shows the RM3c simulated precipitation for the same day. RM3c represents the major features observed by TRMM, including maxima associated with AEWs near 8 and 28°W. Figure 8c shows the precipitation distribution for the RM3ca simulation and Fig. 8d shows the RM3c minus RM3ca precipitation differences. The main RM3c minus RM3ca difference is higher precipitation over the northern third of the Atlantic disturbance by up to 20 mm. RM3c also produces lower orographic precipitation by 10–15 mm along the immediate coast near the Guinea Highlands and higher accumulations over the continent, consistent with the seasonal impacts noted above in reference to Fig. 3. Note that the core precipitation associated with the 8°W disturbance is similar for both simulations.

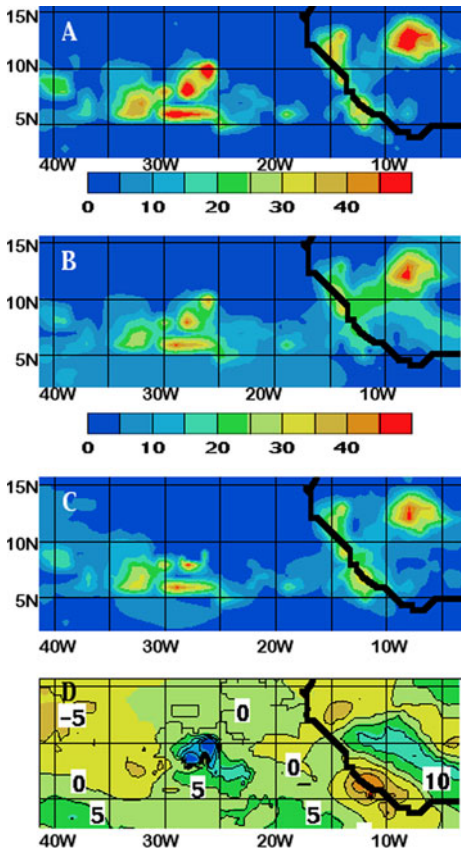

Fig. 8 Precipitation accumulations on 10 September 2006: **a** TRMM (courtesy, NASA GES DISC), **b** RM3c, **c** RM3ca, **d** RM3c minus RM3ca. Units: mm

3.4 Time–latitude variability of JJAS 2006 precipitation

The TRMM time–latitude Hovmoller distribution of daily precipitation rates, averaged over 40–20°W (Fig. 9a), shows that the ITCZ is composed of discreet precipitation events separated with partial or complete breaks. Precipitation maxima appear to move northward with time, creating diagonal swaths. The RM3c simulation (Fig. 9b) recreates many of those swaths, although the simulated breaks are not as sharp as the observed. Moreover, the model simulates light rain between 0 and 3°N during most of the summer, even though TRMM evidence suggests that this low latitude precipitation wanes toward the end of June. The northward course of precipitation maxima is apparently characteristic of tropical Atlantic systems, since the time–latitude precipitation distributions over West Africa show little or no time displacements of individual swaths in the meridional plane (see following discussion of Fig. 10). The timing and location of most TRMM and RM3c maxima match quite well. The starting point of the swaths is close to the equator in early June, while they start farther and farther northward as the season progresses, until the beginning of September. The same systems also propagate westward on time–longitude Hovmöller distributions (Fig. 6), so the total movement is toward the northwest. In late August, swaths begin at about 5°N and ultimately reach about 18°N. RM3c simulates generally higher precipitation rates than RM3ca (Fig. 9c) within the ITCZ, mostly between 0 and 10°N, although positive impacts occasionally extend to 15°N (Fig. 9d). Figure 9d also shows a prominent band of precipitation reduction near 6°N at the end of July into the beginning of August, and several events of slight precipitation reduction during August and September between 12° and 18°N. Druyan et al. (2009) reported less precipitation between 9° and 15°N in an RM3 simulation with September 2006 SST compared to results forced by −3°K SSTA.

The time–latitude distributions of daily precipitation averaged between 0° and 12°W (Fig. 10) show a gradual monsoon onset and gradual retreat. The 5°N latitude divides this domain between the Gulf of Guinea to the south and continental West Africa to the north. Nearly horizontal swaths of heavy precipitation indicate that individual precipitation maxima do not propagate northward or southward with time. RM3c produces a mixture of reductions and enhancements of daily precipitation relative to RM3ca, plotted in Fig. 10c. As over the tropical Atlantic, different SST forcing hardly changes the timing and location of precipitation events and, moreover, there is no detectable SST impact on the monsoon onset or retreat (see also Fig. 11). A distinct precipitation reduction, despite the warmer SST forcing, occurs between 0° and 6°N, along and south of the Gulf of Guinea coastline. The most prominent of these decreases occurs during June and September, when the rain band is centered near the coast, although some decreases are detected at 5°N even in July–August. Enhancement during July reaches as far north as 18°N. The predominant enhancement of precipitation is consistent with higher RM3c evaporation from the Gulf of Guinea and stronger moisture convergence, as discussed above.

The northward advance of precipitation from the Gulf of Guinea coast to the Sahel in early summer is often termed the "onset" of monsoon rains over West Africa. Sultan and Janicot (2000) and Hagos and Cook (2007) suggest that a working definition of onset is the day on which the running mean of precipitation at 10°N first exceeds the running mean at 5°N. Figure 11 graphs 9-day running means of daily precipitation averaged over 0°–12°W (western Sahel) along 5°N and along 10°N for TRMM (Fig. 11a), RM3c (Fig. 11b) and RM3ca (Fig. 11c). Figure 11d shows the RM3c minus RM3ca impacts at those latitudes. Comparison of Fig. 11a, b shows that RM3c running means of daily precipitation are correlated with corresponding TRMM time variability: $r = 0.93$ at 5°N, but only $r = 0.31$ at

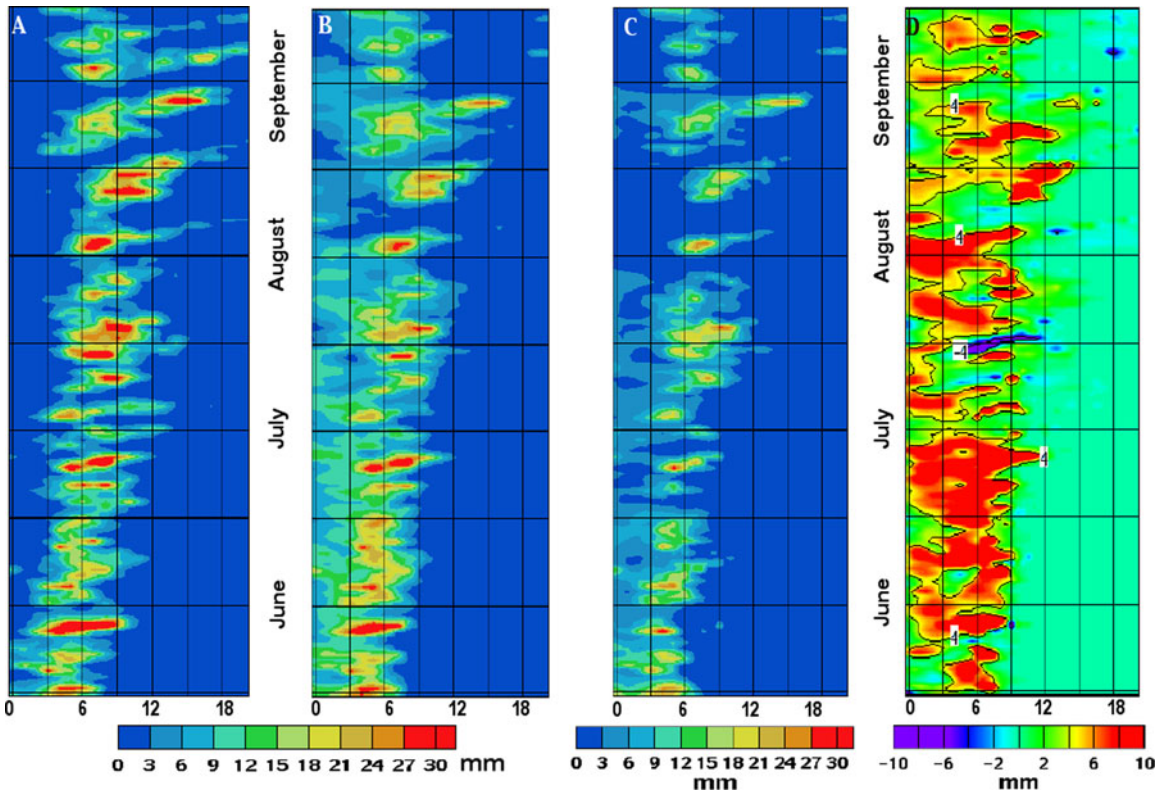

Fig. 9 Time–latitude distributions of daily precipitation (mm) averaged over 20°–40°W: **a** TRMM (courtesy, NASA GES DISC), **b** RM3c, **c** RM3ca, **d** RM3ca minus RM3c (contour shows differences > +4 mm)

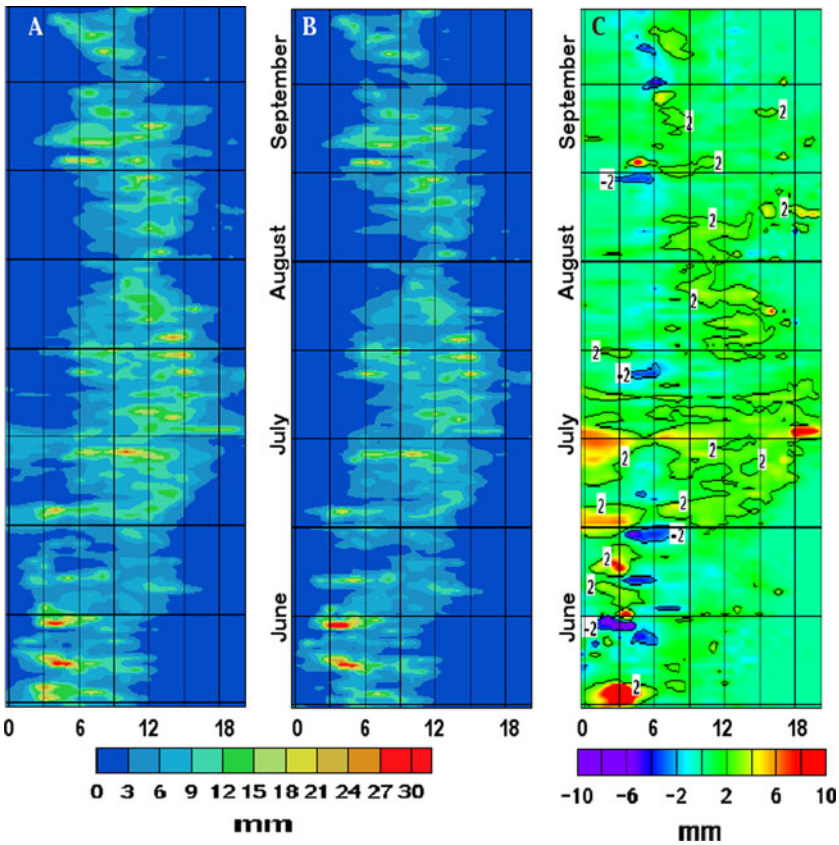

Fig. 10 Time–latitude distributions of daily precipitation (mm) averaged over 0°–12°W: **a** RM3c, **b** RM3ca, **c** RM3ca minus RM3c (contour shows differences > +4 mm)

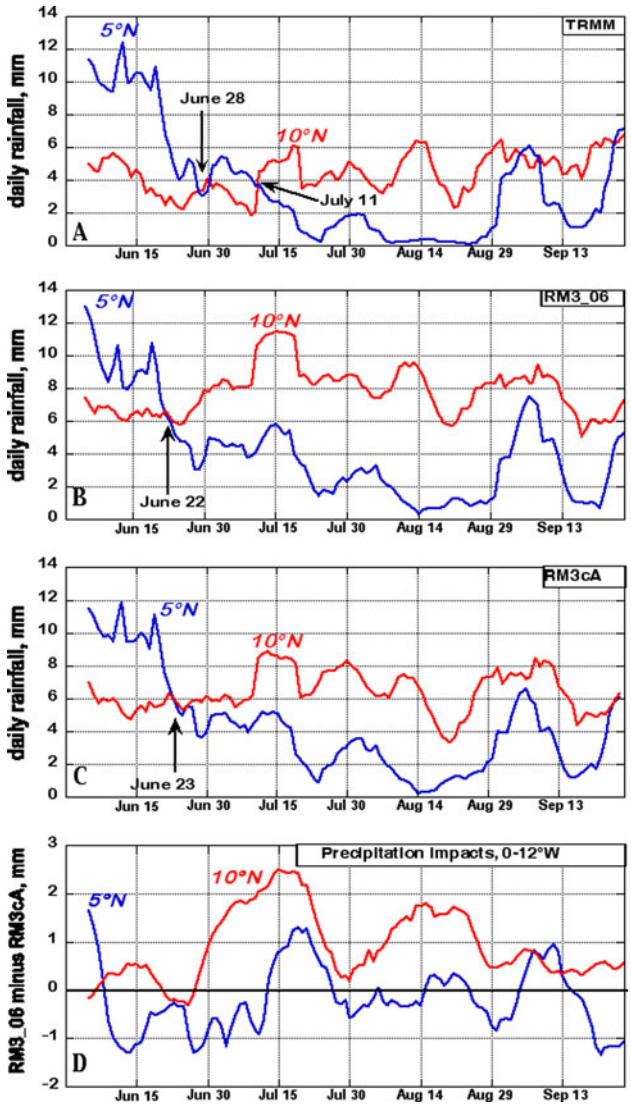

Fig. 11 Nine-day running means of simulated precipitation along 5°N and 10°N, averaged over 0°–12°W for **a** RM3c; **b** RM3ca and **c** RM3ca minus RM3c impacts

10°N, where modeled values are consistently higher between 30 June–13 September. However, both correlations are statistically significant at the 99% confidence level. Onset based on TRMM data occurs on 28 June, for RM3c on 22 June and for RM3ca on 23 June. Figure 11d shows that RM3c reduces precipitation at 5°N during parts of June, early July and September. However, RM3c simulates consistently more precipitation than RM3ca at 10°N during July–September. Most importantly, the inclusion of the eastern tropical Atlantic SST maximum hardly changes the monsoon onset date.

The time–latitude distribution of RM3c daily precipitation averaged between 12° and 20°W (Fig. 12a) depicts higher precipitation rates than between 0° and 12°W. Note that this longitudinal interval includes the Atlantic coastline of Africa. The center of the rain band moves from about 6°N in June to about 8°N in July and individual swaths do not show northward movement as over the open ocean. Neither the timing of main precipitation events nor the onset and retreat seem to have been affected by the different SST specifications (compare Fig. 12a, b). The largest and most sustained positive impacts of the warmer SST on simulated daily precipitation (Fig. 12c) are between 0° and 5°N, which is the southern edge of the rain band. Within the rain band, positive impacts are interdispersed with occasional reductions. Large reductions forced by the inclusion of the eastern tropical Atlantic SST maximum occur within the center of the rain band in mid-July, for three events in August and during much of September. Figures 3c and 8d suggest that these reductions are somehow related to orographic precipitation along the coast near the Guinea Highlands.

3.5 Impacts on precipitation spectra

Organization of precipitation maxima by transient disturbances, such as AEWs, can create periodicities in precipitation that are detected by fast Fourier spectral analysis of precipitation time series at selected locations. Druyan et al. (2006) show a strong spectral peak with approximately 5-day period for an RM3 simulated time series of daily precipitation during JJAS 2002 over West Africa. Figure 13a shows the power spectrum of RM3c time series of daily precipitation during JJAS 2006 at 10°N, 25°W (over the Atlantic). Since precipitation sampling is daily, periods shorter than 2 days are not resolved and that part of the spectrum is ignored. The RM3c spectrum includes a statistically significant peak at the 2.5-day period, and a weaker, non-significant peak at 4.0 days. Since 2.5 days is so close to the shortest resolvable period, the 2.5-day peak may be an artifact of aliasing and not physically relevant. The 4.0-day peak, however, may be related to AEWs, which show peak periodicities within the 3- to 6-day range based on spectral analysis of meridional wind time series (discussed below). Figure 13b shows the spectrum for the corresponding precipitation data simulated by RM3ca. The 2.5-day peak is about half the amplitude of the original for the RM3ca experiment, but the 4.0-day peak is only slightly diminished. Interestingly, reductions in time variability reduce the threshold for significance, so that the 4.0-day and the 8.0-day peaks for this simulation are statistically significant at the 95% confidence level. The implication is that precipitation time variability caused by AEWs stands out better against the general variability in the more stably stratified regime. In contrast, the near-equator SST maximum induces more frequent and more copious moist convection that masks the significance of transient disturbances. Over West Africa, precipitation

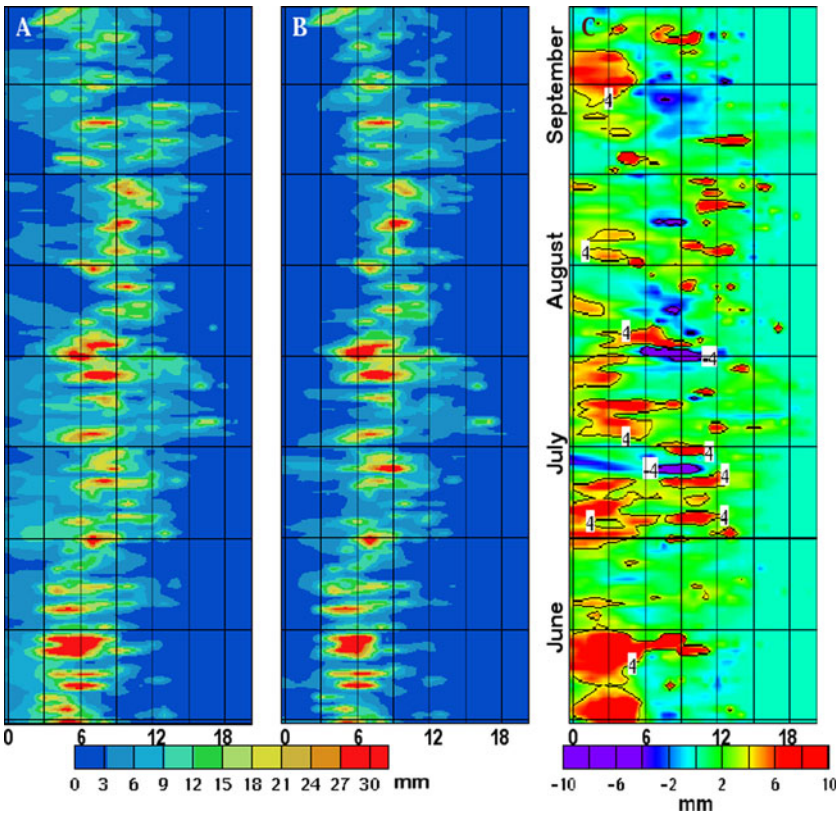

Fig. 12 Time–latitude distributions of daily precipitation (mm) averaged over 12°–20°W: **a** RM3c, **b** RM3ca, **c** RM3c minus RM3ca (contour shows differences > +4 mm)

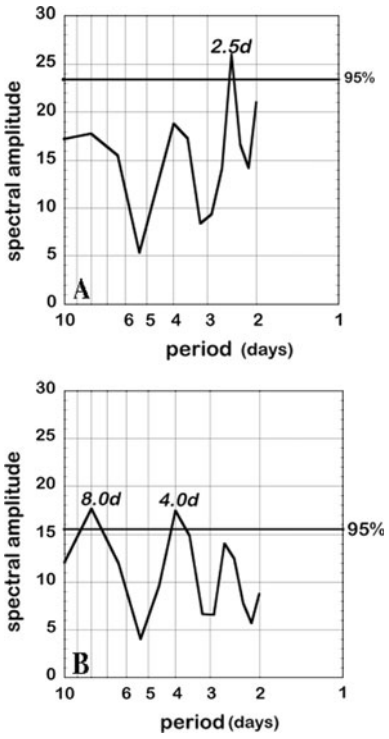

Fig. 13 Spectra of daily precipitation time series during JJAS 2006 at 10°N, 25°W: **a** for RM3c, **b** for RM3cA. The threshold for 95% confidence of statistical significance is shown and the periods of significant peaks are labeled

power spectra are similar for the two experiments (not shown). Moreover, the large time variability of precipitation over land produces time series with no statistically significant peaks in the 3–5 days range in either simulation.

4 SST impacts on thermal vertical stability

Upward motion of air is forced by near-surface convergence even in stable thermal stratification, but warm SST enhances convection. The SST maximum in the eastern tropical Atlantic also creates the near-equatorial sea-level pressure trough (Hastenrath and Polzin 2010), which in turn promotes convergence and forced upward motion. The temperature of the ocean surface affects the thermal stability of the lower troposphere since warm SSTs destabilize the air column by elevating surface air temperatures and cold SSTs have the opposite effect. Figure 14 shows the JJAS average temperature differences between 2 m and 850 mb over the tropical Atlantic for the two simulation experiments. These lapse rates are highly variable in time and follow a pronounced diurnal cycle over land, related to the rapid response of land temperatures to incoming solar radiation, with smaller diurnal variability over the ocean. The axis of maximum lapse rate along 5°N over the eastern tropical Atlantic approximately coincides with the latitude

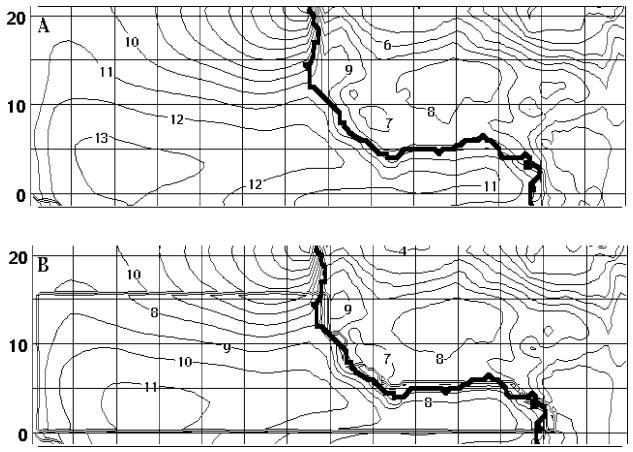

Fig. 14 JJAS mean temperatures at 2 m minus temperatures at 850 mb for **a** RM3c, **b** RM3cA, °K

of maximum convective precipitation within the ITCZ. RM3c features maximum lapse rates of about 13°K, while the RM3ca maximum lapse rate is about 2°K lower due to the prescribed negative SSTA. The dry adiabatic temperature lapse rate between the ocean surface and 850 mb is about 14.5°K and the saturation moist adiabatic lapse rate is about 8°K, so the range of 11–13°K represents a conditionally unstable atmosphere. The larger mean lapse rates of the RM3c simulation create greater buoyant lift for saturated updrafts, and are therefore consistent with larger seasonal precipitation accumulations. However, the relative influences of temperature lapse rates versus moisture convergence are not assessed. Lapse rates over West Africa are approximately the same for both experiments.

5 SST impacts on circulation

Time series of 700-mb meridional wind (*v7)* for the RM3c and RM3ca experiments, respectively, are compared at 16°N, 15°W and 18°N, 25°W (not shown). Amplitudes of *v7* oscillations in RM3c, which includes the eastern tropical Atlantic SST maximum, are greater than for RM3ca, but otherwise the alternative SST forcing does not result in different circulation characteristics. For example, co-located JJAS time series of 4× daily *v7* from RM3c versus RM3ca at these locations have $r = 0.99$ correlations. However, the standard deviations of the time series are larger for the warmer SST forcing, 3.3 ms^{-1} compared with 2.8 ms^{-1} at 16°N, 15°W, and 3.5 ms^{-1} compared with 2.9 ms^{-1} at 18°N, 25°W. Consequently, AEW vorticity maxima traverse the same trajectories with the same timing in the two simulations, albeit at different strengths. In addition, spectra and wavelets show identical periodicities and timing of waves, just higher amplitudes for RM3c.

Figure 15 shows Hovmöller time–longitude distributions of four times daily calculations of the 700-mb relative vorticity during JJAS due to zonal gradients of the meridional wind, $\zeta = \delta v/\delta x$. Thorncroft et al. (2007) represented AEW trajectories by a time–longitude plot of 700-mb curvature vorticity. Here, values of ζ are averaged over 10°–15°N, which is the approximate swath of cyclonic AEWs in this region during JJAS. The second term of relative vorticity, $-\delta u/\delta y$, is strongly positive due to the mean circulation of strengthening easterlies from south to north, so $\zeta = \delta v/\delta x$ alone conveniently monitors the strength of transient AEWs at 700 mb. In Fig. 15, white swaths represent the strongest vorticity, therefore the most intense cyclonic disturbances, while pale gray swaths are weakly cyclonic. Swaths of negative ζ represent the anticyclonic ridges separating AEWs. The diagonal orientation of vorticity swaths indicates westward propagation. Hovmöller distributions of ζ are shown for the RM3c (Fig. 15a) and RM3ca (Fig. 15b) simulations. The vorticity signature for RM3c (Fig. 15a) shows cyclonic disturbances with the same timing and location as RM3ca, but there are several examples of longer trajectories of vorticity maxima and higher intensity. Parallel Hovmöller distributions of divergence in the lower troposphere show corresponding

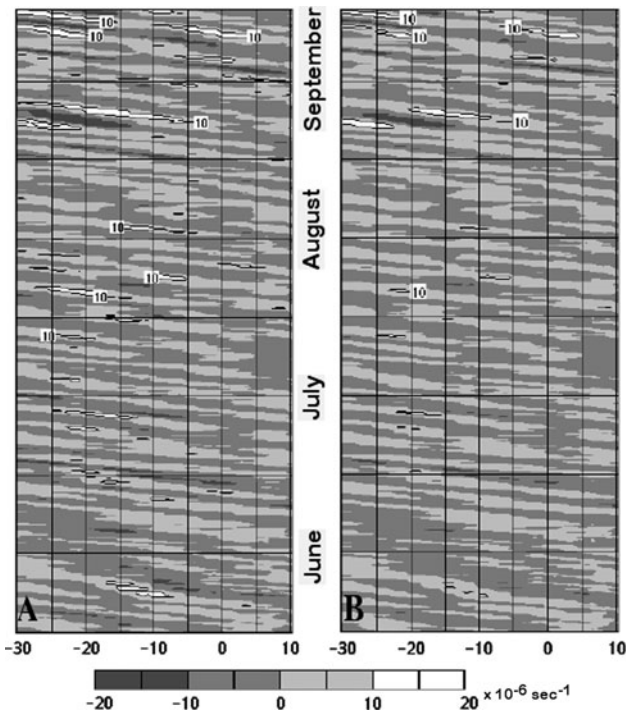

Fig. 15 Time–longitude distribution of four times daily zonal gradient of 700 mb meridional wind, representing relative vorticity, averaged over 10°–15°N. **a** RM3c, **b** RM3ca. Units: $\times 10^{-6}$ s^{-1}. The contours for 10 × 10^{-6} and 20 × 10^{-6} s^{-1} are shown

westward propagating, alternating convergence and divergence swaths, which are stronger for RM3c. Thus, the timing and location of AEW trajectories forced by the common lateral boundary conditions are the same in both experiments, while warmer SST forcing favors more intense AEWs.

Power spectra of JJAS time series of 4× daily *v7* are computed at each grid point of the model domain. Figure 16a shows the spatial distribution of the average spectral amplitude between 3- and 6-day periods for RM3c *v7* spectra over the domain. Maximum amplitudes are centered along 16°–17°N, ranging westward from West Africa to the eastern tropical Atlantic Ocean. A second maximum extends from 35°E to the Gulf of Guinea coast along 5°N. Each maximum implies either frequent AEW activity and/or the traversal of high amplitude AEWs, so the maxima represent storm tracks. Figure 16b–d show RM3c *v7* spectra for three grid elements within the implied storm tracks. The most prominent (and statistically significant) spectral peak at both 18°N, 25°W and 16°N, 15°W is at 4.4 days, representative of typical periods of AEWs (Druyan et al. 1996). In addition, a statistically significant spectral peak is featured at 6.1 days. Diedhiou et al. (1999) find that 6- to 9-day period waves in NCEP and ECMWF reanalysis data are strongest over West Africa north of 20°N. At 5°N, 5°W, three spectral peaks are evident between 3 and 4 days, but amplitudes are lower than over 16°–18°N. The spatial distribution of spectral amplitude between 3- and 6-day periods, created for *v7* spectra from the RM3ca experiment, is the same as in the RM3c case (not shown), but the maximum amplitude is 10–15% lower. Figure 16e shows the *v7* spectra at 16°N, 15°W for RM3ca (compare to Fig. 16c). Significant spectral peaks occur at the same periods as for RM3c, but amplitudes are about 15% lower.

Wavelets for the *v7* time series at 16°N, 15°W and 18°N, 25°W (not shown) indicate strong and significant maxima at 4- to 5-day periods during mid-July and the second half of August. A third maximum occurs between 3- and 4-day periods toward the middle of September, corresponding to the traversal of the pre-Helene storm. Differences between the wavelets at 15°W and 25°W reflect the evolving pattern due to wave development or weakening. For example, two significant maxima detected at 16°N, 15°W (late June and early August, respectively) do not survive as significant amplitudes reaching 25°W, but both late summer systems intensify. Wavelets based on *v7* data from RM3c show significant maxima with identical timing and periodicity as results from RM3ca *v7*, except that maximum amplitudes are increased by 10–35%, consistent with the wind speed and spectral amplitude amplifications mentioned above.

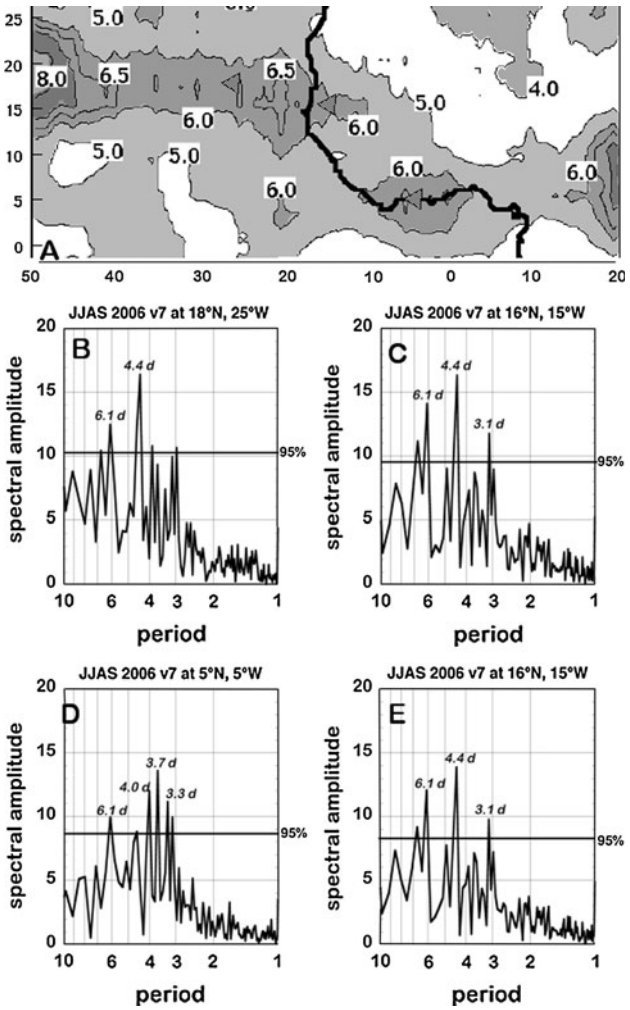

Fig. 16 **a** Spatial distribution of average spectral amplitude between 3- and 6-day periods, of RM3c *v7* JJAS time series, **b** power spectrum of RM3c *v7* JJAS time series at 18°N, 25°W, **c** power spectrum of RM3c *v7* JJAS time series at 16°N, 15°W, **d** power spectrum of RM3c *v7* JJAS time series at 5°N, 5°W, **e** power spectrum of RM3ca *v7* JJAS time series at 16°N, 15°W

6 Discussion and conclusions

Two RM3 simulations over West Africa and the adjacent tropical Atlantic are forced with NCPR2 boundary conditions, 15 May–6 October 2006, in essence downscaling NCPR2 to a 0.5° grid. Dynamic downscaling is especially helpful in this region where precipitation events are associated with African easterly waves (AEWs) and squall lines. The first ("basic") simulation uses NCPR2 2006 SST, while the second assesses the consequences of eliminating the eastern tropical Atlantic SST maximum by subtracting 3°K from all SST between 0 and 15°N throughout the simulation. The basic simulation reproduces the major JJAS 2006 mean precipitation features, as estimated by TRMM, over the eastern tropical Atlantic and the Guinean and Cameroon Highlands, although RM3

accumulations over West Africa are otherwise about 25% higher than TRMM. Estimated JJAS moisture convergence above a representative maritime sampling region is 133% higher as a consequence of the tropical Atlantic SST maximum, which also enhances local rainfall by decreasing vertical thermal stability. JJAS rainfall is increased by 74% over the sampled ocean area owing to the warm SST. An example from observational data sets comparing two different seasons shows that the season with 1.0°K higher SST under the eastern Atlantic ITCZ experiences 35% more JJAS precipitation.

The basic simulation generates realistic time–longitude swaths of precipitation maxima associated with westward propagating AEWs. Forcing with a realistic SST maximum is shown to generally increase the maximum precipitation rates of these swaths over the ocean, some of which are even eliminated by the cold SST specification. However, timing and position of tracks are never altered by the alternate SST boundary conditions. In the example of the eastern tropical Atlantic storm on 10th September, results with the cold SSTs included a considerably truncated precipitation shield. Precipitation differences between the two simulations are less dramatic over West Africa.

Time–latitude distributions of daily rainfall over the tropical Atlantic imply northwesterly movement of precipitation maxima throughout the summer. The eastern tropical Atlantic SST maximum accounts for precipitation enhancements mostly between 0° and 10°N, with occasional positive impacts farther north. Several episodes of precipitation decreases, despite warmer SSTs, are also featured.

The onset of monsoon rains over West Africa is computed here as the earliest date on which 9-day running means of precipitation at 10°N first exceed the corresponding value at 5°N. The onset simulated with realistic forcing occurs about 6 days earlier than according to TRMM estimates using this definition, because TRMM and model time series over 10°N are only loosely correlated. Simulation results show that alternate SSTs in the eastern tropical Atlantic and Gulf of Guinea change the onset date by only 1 day. The warm SSTs occasionally reduce rainfall along the West African coast near 5°N during the course of the summer, but increase daily rates at 10°N during much of July–August.

Simulated time series of rainfall over the eastern tropical Atlantic show a peak periodicity near 4 days, reflecting the organization of maxima by AEWs. The 4-day peak is not statistically significant based on 2006 SST forcing, but that simulation does produce a statistically significant periodicity at 2.5 days. Removing the eastern tropical Atlantic SST maximum lowers the threshold for statistical significance by decreasing time variability of precipitation. For example, the standard deviation of the precipitation time series at 10°N, 25°W is reduced by 34%. While the warm SSTs double the 2.5 days spectral peak, they have little effect on the amplitude of the 4-day peak, which is statistically significant only for the cold SST forcing. Results suggest that the near-equatorial SST maximum causes high-frequency time variability of moist convective rainfall, while atmospheric forcing from West Africa, not very sensitive to SST, regulates 4-day periodicity via the influence of AEWs.

Time series of meridional wind at 700 mb ($v7$) feature strong, statistically significant spectral peaks at 4.4-day periods, associated with AEWs. Alternate SSTs do not change the periodicity, but the SST maximum does increase the amplitude of spectral peaks by about 20%, consistent with increases in the amplitude of $v7$ time variability. Both simulations produce the same swaths of westward propagating vorticity, but vorticity maxima are stronger in the basic run, owing to the stronger circulation.

The RM3 simulation of the JJAS 2006 evolution of weather and climate over West Africa and the eastern tropical Atlantic is realistic enough to evaluate the sensitivity of the actual climate to alternate specifications of SST in the eastern tropical Atlantic, although model biases must be taken into consideration. Results show that the SST maximum in the eastern tropical Atlantic acutely influences in situ precipitation rates by boosting moisture convergence and reducing vertical thermal stability. This provides one explanation for the mutual interaction between SSTs and Atlantic ITCZ rainfall discussed by Xie and Carton (2004). The study implies that transient easterly waves and incipient tropical cyclones in the eastern tropical Atlantic owe some of their intensity to the SST maximum. Rainfall rates over the Sahel are also enhanced by greater moisture convergence over West Africa afforded by warmer SST in the Gulf of Guinea, but SST have minimal impact on wave circulation over land. The timing and trajectories of AEWs are not affected by SSTs, but seem to be uniquely determined by the atmospheric and surface boundary conditions that were common to the two simulations.

Acknowledgments This research was supported by National Science Foundation grants AGS-0652518 and AGS- 0652518, National Aeronautics and Space Administration (NAMMA) grant NNX07A193G and the National Aeronautics and Space Administration Climate and Earth Observing System Program. TRMM data were acquired using the GES DISC Interactive Online Visualization and Analysis Infrastructure (Giovanni) as part of NASA's Goddard Earth Sciences (GES) Data and Information Services Center (DISC). NCEP reanalysis 2 data were obtained online from the National Oceanographic and Atmospheric Agency/Earth System Research Laboratory (Physical Sciences Division). We gratefully acknowledge the three anonymous reviewers who made suggestions that contributed significantly to the final version of the paper.

References

Burpee R (1972) The origin and structure of easterly waves in the lower troposphere of North Africa. J Atmos Sci 29:77–90

Chiang JCH, Kushnir Y, Giannini A (2002) Deconstructing Atlantic ITCZ variability: influence of the local cross-equatorial SST gradient, and remote forcing from the eastern equatorial Pacific. J Geophys Res 107 (D1):4004. doi:10.1029/2000JD000307

Del Genio A, Yao M-S (1993) Efficient cumulus parameterization for long-term climate studies. In: Emanuel K, Raymond D (eds) The GISS scheme. Cumulus Parameterization, Am Meteorol Soc Monogr Ser (Boston). 24:181–184

Del Genio A, Yao M-S, Kovari W, Lo K-W (1996) A prognostic cloud water parameterization for global climate models. J Clim 9:270–304

Diedhiou A, Janicot S, Viltard A, de Felice P, Laurent H (1999) Easterly wave regimes and associated convection over West Africa and tropical Atlantic: results from NCEP/NCAR and ECMWF reanalyses. Clim Dyn 15:795–822

Druyan L, Lonergan P, Saloum M (1996) African wave disturbances and precipitation at Niamey during July–August 1987 and 1988. Clim Res 7:71–83

Druyan L, Fulakeza M, Lonergan P (2006) Mesoscale analyses of West African summer climate: focus on wave disturbances. Clim Dyn 27:459–481. doi:10.1007/s00382-006-0141-9

Druyan L, Fulakeza M, Lonergan P (2008) The impact of vertical resolution on regional model simulation of the west African summer monsoon. Int J Climatol 28:1293–1314

Druyan L, Fulakeza M, Lonergan P, Noble E (2009) Regional climate model simulation of the AMMA special observing period #3 and the pre-Helene easterly wave. Meteorol Atmos Phy 103:191–210

Druyan L, Feng J, Cook K, Xue Y, Fulakeza M, Hagos S, Konaré A, Moufama-Okia W, Rowell D, Vizy E, Ibrah S (2010) The WAMME regional model intercomparison study. Clim Dyn 35:175–192. doi:10.1007/s00382-009-0676-7

Folland CK, Palmer T, Parker D (1986) Sahel rainfall and worldwide sea temperatures, 1901–85. Nature 320:602–607

Giannini A, Saravanan R, Chang P (2003) Oceanic forcing of Sahel rainfall on interannual to interdecadal time scales. Science 302:1027–1030

Hagos S, Cook K (2007) Dynamics of the West African Monsoon Jump. J Clim 20:5264–5284

Hansen J et al (2002) Climate forcings in Goddard Institute for Space Studies SI2000 simulations. J Geophys Res 107:4347. doi:10.1029/200IJD001143

Hastenrath S, Polzin D (2010) Long-term variations of circulation in the tropical Atlantic sector and Sahel rainfall. Int J Climatol. doi:10.1002/joc.2116.

Hopsch S, Thorncroft C, Hodges K, Aiyyer A (2007) West African storm tracks and their relationship to Atlantic tropical cyclones. J Clim 20:2468–2483

Hopsch S, Thorncroft C, Tyle K (2010) Analysis of African easterly wave structures and their role in influencing tropical cyclogenesis. Mon Wea Rev 138:1399–1419

Kanamitsu M, Ebisuzaki W, Woollen J, Yang S-K, Hnilo J, Fiorino M, Potter G (2002) NCEP-DEO AMIP-II Reanalysis (R-2). Bull Am Meteorol Soc 83:1631–1643

Reed R, Norquist D, Recker E (1977) The structure and properties of African wave disturbances as observed during Phase III of GATE. Mon Wea Rev 105:317–333

Reed R, Klinker E, Hollingsworth A (1988) The structure and characteristics of African easterly wave disturbances as determined from the ECMWF operational analysis/forecast system. Meteorol Atmos Phys 38:22–33

Rosenzweig C, Abramopoulos F (1997) Land-surface model development for the GISS GCM. J Clim 10:2040–2054

Ross R, Krishnamurti T (2007) Low-level African easterly wave activity and its relation to Atlantic tropical cyclogenesis in 2001. Mon Wea Rev 135:3950–3964

Rowell DP (2001) Teleconnections between the Tropical Pacific and the Sahel. Q J R Meteorol Soc 127:1683–1706

Rowell DP (2003) The impact of Mediterranean SSTs on the Sahelian rainfall season. J Clim 16:849–862

Sultan B, Janicot S (2000) Abrupt shift of the ITCZ over West Africa and intra-seasonal variability. Geophys Res Lett 27:3353–3356

Thorncroft C, Hodges K (2001) African easterly wave variability and its relationship to Atlantic tropical cyclone activity. J Clim 14:1166–1179

Thorncroft C, Lafore J, Berry G, Roca R, Guichard F, Tomasini M, Asencio N (2007) Overview of African weather systems during the summer 2006. CLIVAR Exchanges 12:18–20

Woolings T, Hoskins B, Blackburn M, Hassell D, Hodges K (2010) Storm track sensitivity to sea surface temperature resolution in a regional atmosphere model. Clim Dyn 35:341–353

Xie S-P, Carton JA (2004) Tropical Atlantic variability: patterns, mechanisms, and impacts. In: Wang C, Xie S-P, Carton JA (eds) Ocean–atmosphere interaction and climate variability. AGU Press, USA